JOURNAL OF AIRCRAFT
Vol. 40, No. 4, July–August 2003

Natural-Laminar-Flow Airfoil Development for a Lightweight Business Jet

Michimasa Fujino,* Yuichi Yoshizaki,† and Yuichi Kawamura‡
Honda R&D Americas, Inc., Greensboro, North Carolina 27409

A 15% thick, natural-laminar-flow airfoil, the SHM-1, has been designed to satisfy requirements derived from the performance specifications for a lightweight business jet. The airfoil was tested in a low-speed wind tunnel to evaluate its low-speed performance. A flight test was also conducted to evaluate the performance of the airfoil at high Reynolds numbers and high Mach numbers. In addition, a transonic wind-tunnel test was conducted to determine the drag-divergence characteristics. The design requirements, methodology, and experimental verification are described.

Nomenclature

C_d	=	section profile drag coefficient
C_l	=	section lift coefficient
$C_{l\max}$	=	section maximum lift coefficient
C_m	=	section pitching moment coefficient about quarter-chord point
C_p	=	pressure coefficient
$C_{p,\text{sonic}}$	=	critical pressure coefficient
c	=	airfoil chord, m
M	=	Mach number
M_{DD}	=	drag-divergence Mach number, Mach number at which $\mathrm{d}(C_d)/\mathrm{d}M = 0.1$
n	=	amplification factor for transition prediction
Re	=	Reynolds number based on freestream conditions and airfoil chord
x	=	airfoil abscissa, m
x_T	=	transition location, m
α	=	angle of attack relative to chord line, deg

Introduction

THE business jet is becoming a common tool for business people. In particular, the small business jet that is more efficient in operation is expected to become more popular. To improve the efficiency of such aircraft, it is very important to reduce drag. The natural-laminar-flow (NLF) airfoil is considered to be one of the key technologies to reduce drag and, thus, improves performance significantly.

Many NLF airfoils have been developed in the past. For example, in the early 1940s, NACA developed the 6-series airfoils[1] that have appeal because of their low drag. For the 6-series airfoils, however, the loss of laminar flow due to leading-edge contamination sometimes causes a significant reduction in the maximum lift coefficient, which creates a very dangerous situation during takeoff or landing. This is a particularly undesirable characteristic for business jets for which safety is a prime concern.

Presented as Paper 2002-2932 at the AIAA 20th Applied Aerodynamics Conference, St. Louis, Missouri, 24 June 2002; received 5 November 2002; revision received 3 March 2003; accepted for publication 5 March 2003.

*Chief Engineer, 6423B Bryan Boulevard; fujinox@alles.or.jp. Member AIAA.
†Assistant Chief Engineer, 6423B Bryan Boulevard; yyoshizaki@oh.hra.com.
‡Research Engineer, 6423B Bryan Boulevard; ykawamura@oh.hra.com. Member AIAA.

More recently, NASA has designed several advanced NLF airfoils such as the NLF(1)-0215F airfoils[2] and NLF(1)-0414F airfoils,[3,4] etc. Although these airfoils achieve low drag, they are intended for low-speed applications. They also exhibit large nose-down pitching moments and low drag-divergence Mach numbers, which are not suited to business-jet applications.

One example of an NLF airfoil suitable for business-jet applications is the NASA HSNLF(1)-0213 airfoil.[4–6] This airfoil has a high drag-divergence Mach number and small nose-down pitching moment. Its maximum lift coefficient at low Reynolds numbers is, however, relatively low. In addition, its 13% thickness limits the volume of fuel that can be carried in the wing.

To maximize the aircraft performance, an NLF airfoil has been designed to match exactly the requirements of the Honda jet. The airfoil, the SHM-1, exhibits a high drag-divergence Mach number, small nose-down pitching moment, and low drag for high cruise efficiency. It not only achieves a high maximum lift coefficient but also exhibits the docile stall characteristics and insensitivity of the maximum lift coefficient to leading-edge contamination that are crucial for safety, which is extremely important for business jets. The thickness of the airfoil is 15% chord and, therefore, the required fuel can be carried in the wing without increasing the wing area, which would otherwise result in a drag increase.

Design

Requirements

Honda R&D is developing a lightweight business jet. The goals of the Honda jet are to achieve a larger cabin, lower fuel consumption, and higher speed than existing business jets. The maximum takeoff weight of the aircraft is about 9000 lbf (4082 kg). The airfoil design requirements derived from the goals for the Honda jet are as follows.

1) Low section profile drag coefficients are desired at $C_l = 0.26$ for $Re = 11.7 \times 10^6$ and $M = 0.69$ (a cruise condition) and at $C_l = 0.35$ for $Re = 13.6 \times 10^6$ and $M = 0.310$ (a climb condition). To provide some operational margin, the lower limit of the low-drag range was set to $C_l = 0.18$. Thus, low profile drag is desired over the range from $C_l = 0.18$ for $Re = 11.7 \times 10^6$ and $M = 0.690$ to $C_l = 0.35$ for $Re = 13.6 \times 10^6$ and $M = 0.310$. For this application, cruise performance is more important than climb performance, and so more emphasis was placed on low drag at cruise conditions.

2) The section maximum lift coefficient with no flap deflection should be at least 1.6 for $Re = 4.8 \times 10^6$ and $M = 0.134$. The loss in maximum lift coefficient due to leading-edge contamination should be less than 7%. The stall characteristics should be docile.

3) The section pitching moment coefficient should no more negative than -0.04 at $C_l = 0.38$ for $Re = 7.93 \times 10^6$ and $M = 0.70$ to minimize the trim-drag penalty at high altitude and high Mach number cruise condition. In addition, the hinge moment coefficient, that is, aileron floating tendency, should not be excessive.

4) The airfoil thickness must be 15% chord to ensure sufficient fuel volume to satisfy the range requirement.

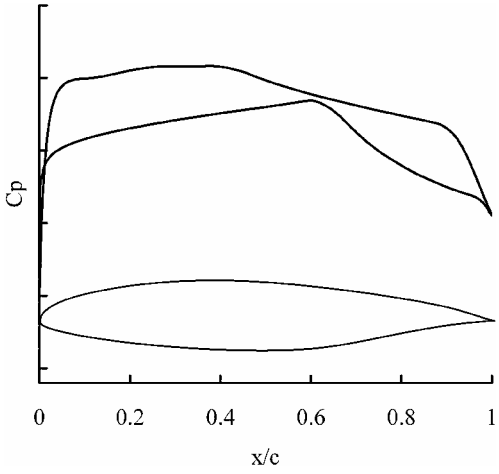

Fig. 1 SHM-1 airfoil shape and pressure distribution.

5) The drag-divergence Mach number should be higher than 0.70 at $C_l = 0.38$.

Methodology

The design was performed using the Eppler airfoil design and analysis code.[7,8] This method, which is based on conformal mapping, allows each segment of the airfoil to be designed independently for different conditions. For example, the upper surface can be designed to maintain laminar flow at the upper limit of the low-drag range and the lower surface can be designed at the lower limit of the low-drag range. The design airfoil was then analyzed and modified to improve $C_{l\,\max}$ and high-speed characteristics using the MCARF and MSES codes.[9,10] The MCARF code contains a two-dimensional, subsonic, panel method; viscous effects are accounted for by altering the geometry of the airfoil to include the displacement thickness obtained from the integral boundary-layer method. The MCARF code was used to evaluate a geometry modification to the airfoil and also for a transition-location study. The MSES code contains an Euler method that solves a streamline-based Euler discretization and a two-equation integral boundary-layer formulation simultaneously using a full Newton method. The MSES code was used to evaluate the high-speed characteristics of the airfoil, including shock formation and drag divergence.

Features of the SHM-1 Airfoil

Figure 1 shows the shape of the SHM-1 airfoil and a representative pressure distribution. The pressure gradient along the upper surface is favorable to about 42% chord, followed by a concave pressure recovery, which represents a compromise between maximum lift, pitching moment, and drag divergence. The pressure gradient along the lower surface is favorable to about 63% chord to reduce drag. A steeper concave pressure recovery was used on the lower surface. The leading-edge geometry was carefully designed to cause transition near the leading edge at high angles of attack to minimize the loss in maximum lift coefficient due to roughness. The upper-surface trailing-edge geometry was designed to produce a steep adverse pressure gradient that confines the movement of separation at high angles of attack and produces a high maximum lift coefficient at the low-speed condition.[11]

It is a critical requirement for high-speed aircraft to reduce the magnitude of the pitching moment coefficient of the airfoil. To reduce the magnitude of the pitching moment coefficient at cruise, the upper-surface geometry was refined to induce a small separation near the trailing edge. By the incorporation of this new trailing-edge design, the magnitude of the pitching moment was greatly reduced. The drag penalty caused by this separation is negligible because the separation is short and shallow.

Experimental Methodology

Low-Speed Wind-Tunnel Test

A low-speed wind-tunnel test was conducted in the Honda 5×3.5 m low-speed wind tunnel to evaluate the low-speed characteristics of the SHM-1 airfoil. A full-scale, two-dimensional model containing 94 static-pressure orifices on the upper and lower surfaces was used to measure the lift and pitching moment coefficients. The profile drag coefficient was measured using a wake rake. The model was tested with transition free and fixed to determine the loss in maximum lift coefficient and the stall characteristics for the leading-edge-contaminated condition. To evaluate the effect of manufacturing tolerances, the actual wing structure was also tested in the wind tunnel (Fig. 2).

Fig. 2 Actual wing structure in Honda low-speed wind tunnel.

Fig. 3 T-33 aircraft modified for NLF flight test.

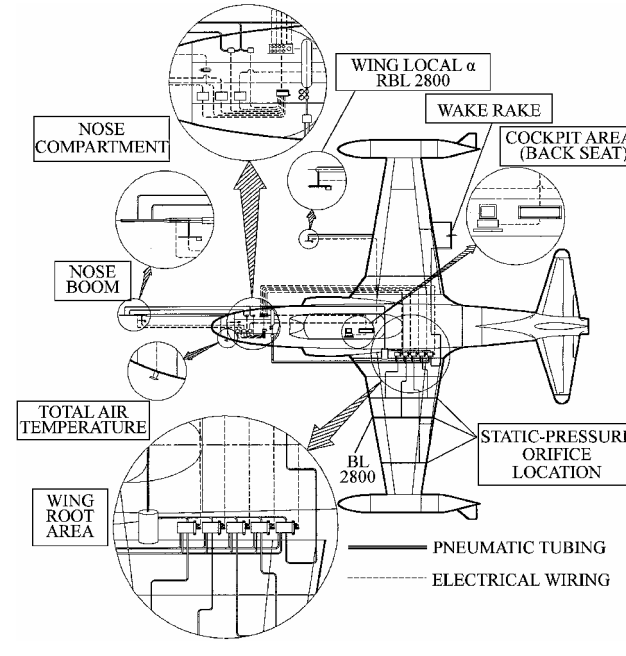

Fig. 4 NLF flight-test instrumentation.

Fig. 5 IR camera in T-33 cockpit.

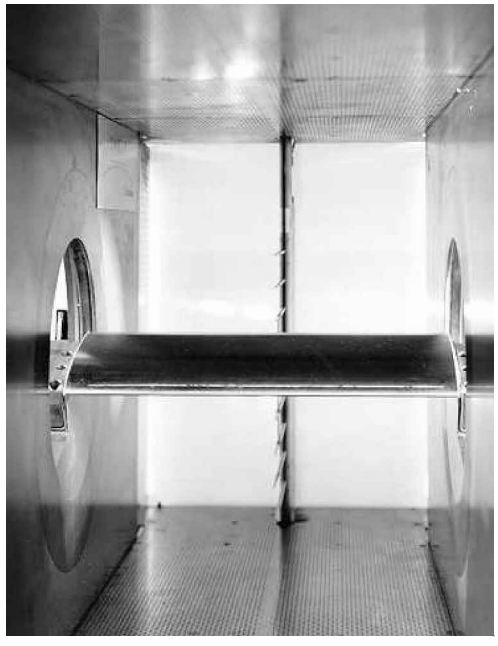

Fig. 6 SHM-1 airfoil model in ONERA transonic wind tunnel.

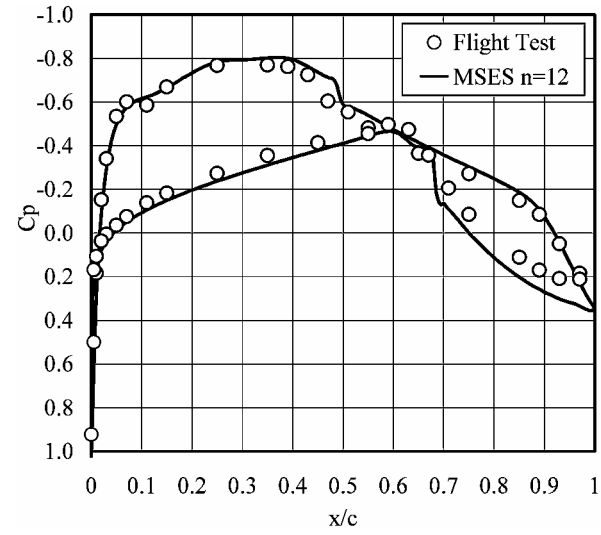

a) $\alpha = 0.27$ deg, $Re = 13.6 \times 10^6$, and $M = 0.62$

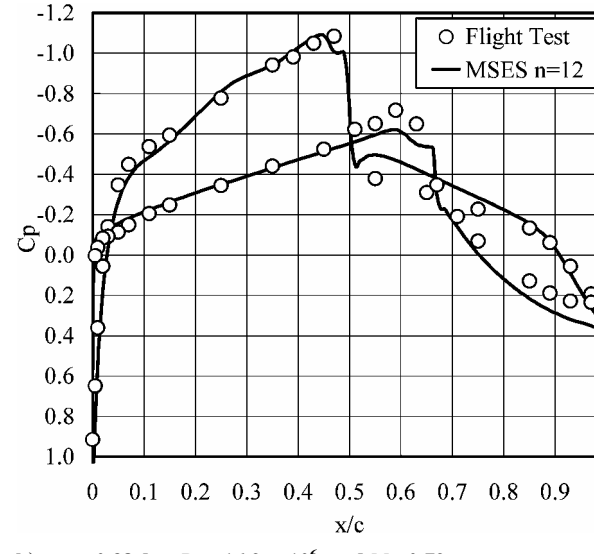

b) $\alpha = -0.38$ deg, $Re = 16.2 \times 10^6$, and $M = 0.72$

Fig. 7 Comparison of theoretical and experimental (flight) pressure distributions.

Flight Test

To evaluate the performance of the SHM-1 airfoil at full-scale Reynolds numbers and high Mach numbers, a flight test was conducted using a modified T-33 aircraft (Fig. 3). The entire wing was modified by bonding polyurethane foam to the original metal wing and then covering the foam with a fiberglass skin. This glove incorporated 119 static-pressure orifices on the upper and lower surfaces at three spanwise stations (Fig. 4). A wake rake was mounted behind the wing trailing edge. An infrared (IR) camera was used to visualize the laminar-to-turbulent boundary-layer transition (Fig. 5). The effect of steps and surface roughness were also investigated.

Transonic Wind-Tunnel Test

To evaluate the high-speed characteristics of the SHM-1 airfoil, a transonic wind-tunnel test was conducted in the ONERA 0.56×0.78 two-dimensional, transonic wind tunnel (Fig. 6). The Mach number was varied from 0.5 to 0.83 and the Reynolds number from 6 to 8×10^6. The drag-divergence characteristics were measured and the shock-wave formation was also investigated using the color schlieren technique.

Results

Pressure Distributions

Figure 7 shows comparisons between two pressure distributions measured in flight and the MSES predictions. The agreement is good for both the subcritical and supercritical cases. The MSES code captures accurately the shock location for the high Mach number condition.

Transition Location

Figure 8 shows an image from the IR camera installed in the T-33 aircraft. By the adjustment of the temperature range from the cockpit, an image that clearly shows the transition location can be obtained. The movement of transition with angle of attack or due to contamination can be observed in real time, which is very helpful for understanding the transition phenomena at various conditions. Figure 9 shows the transition locations obtained using the IR technique. The experimental results and the MCARF predictions agree well. The Eppler code[7,8] predicts earlier transition, whereas the MSES code predicts later transition. The amplification factor n of 12 used in the MSES analysis was selected based on previous correlations. A lower value of this factor would improve the agreement.

Lift

Figure 10 shows the section lift curves obtained from the low-speed wind-tunnel test for $Re = 2.8 \times 10^6$, 4.8×10^6, and 8.0×10^6. The measured maximum lift coefficient is 1.66 for $Re = 4.8 \times 10^6$, which is in good agreement with the prediction of the maximum lift coefficient by the Eppler code.[7,8]

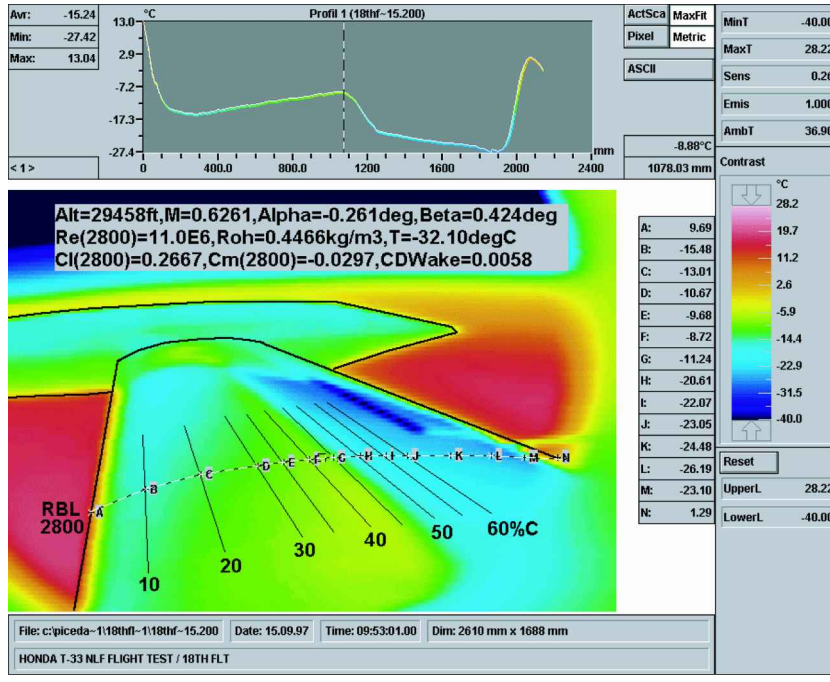

Fig. 8 In-flight transition measurement using IR flow-visualization technique.

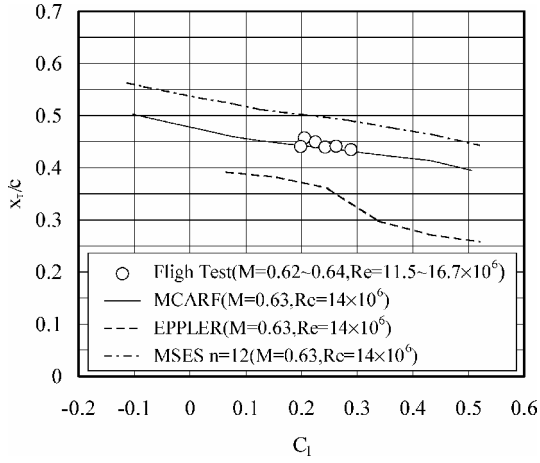

Fig. 9 Comparison of theoretical and experimental (flight) transition locations.

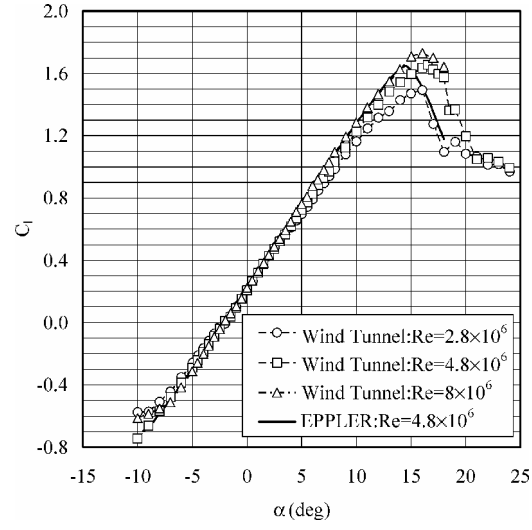

Fig. 10 Comparison of theoretical and experimental (low-speed wind tunnel) lift curves.

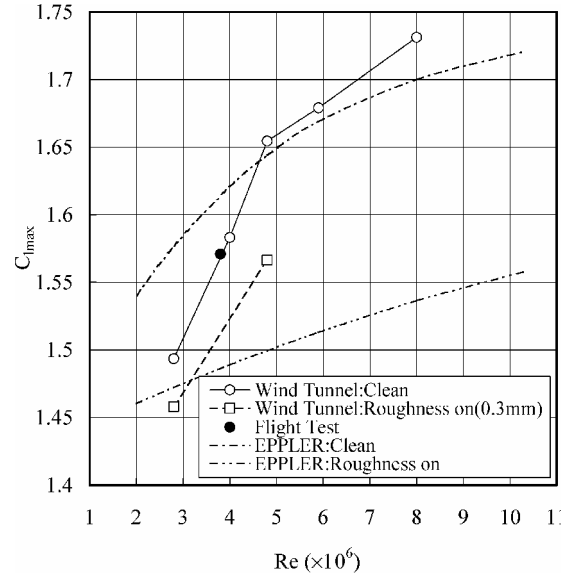

Fig. 11 Effect of Reynolds number on maximum lift coefficient.

Figure 11 shows the effect of Reynolds number on the maximum lift coefficient. The effect on $C_{l\,\max}$ is larger than predicted by the Eppler code.[7,8] Also shown is the effect of leading-edge roughness on the maximum lift coefficient. A 0.3-mm-high trip strip was installed on the upper surface at 5% chord. The critical trip height was determined using the IR flow-visualization technique. The loss in maximum lift coefficient is 5.6% compared to the transition-free condition for $Re = 4.8 \times 10^6$. The loss is less than that predicted by the Eppler code. The design requirements for the maximum lift coefficient and the loss in maximum lift coefficient due to leading-edge contamination were both satisfied.

Drag

Figures 12 and 13 show section profile drag coefficients obtained from the flight test. The conditions shown in Figs. 12a and 12b are near a typical cruise condition. Note that the Reynolds number and Mach number of the flight test were varied as indicated in Fig. 12, but the theoretical prediction was for a representative

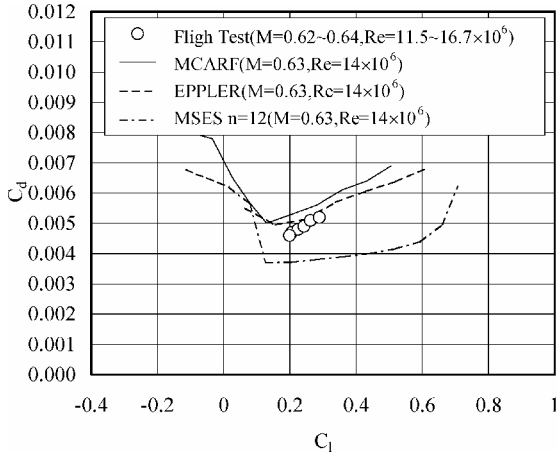

a) $Re = 11.5–16.7 \times 10^6$ and $M = 0.62–0.64$

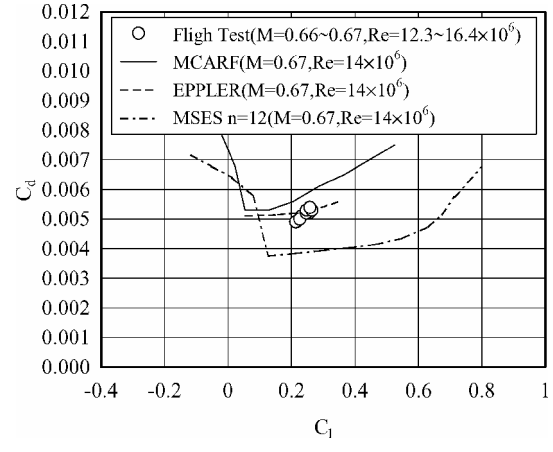

b) $Re = 12.3–16.4 \times 10^6$ and $M = 0.66–0.67$

Fig. 12 Comparison of theoretical and experimental (flight) drag polars.

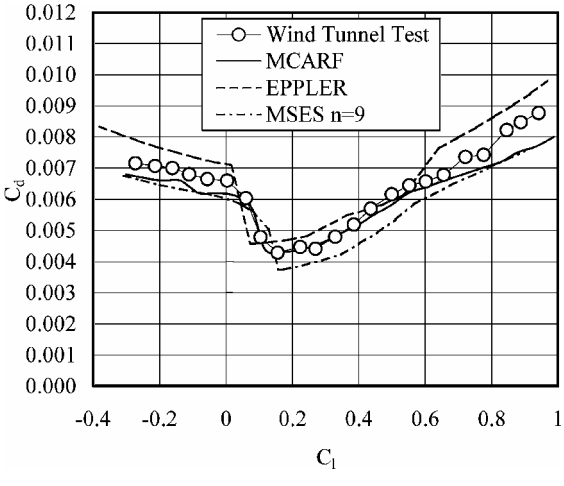

Fig. 13 Comparison of theoretical and experimental (low-speed wind tunnel) drag polars for $Re = 10.3 \times 10^6$ and $M = 0.27$.

Reynolds number and Mach number. The measured drag coefficients are slightly lower than those predicted by the Eppler[7,8] and MCARF codes. Note, however, that neither code accounts for wave drag, which is estimated to contribute 4–5 counts at $M = 0.63$ or about 7 counts at $M = 0.67$. The MSES code underpredicts the drag, even though it includes the wave-drag contribution. This underprediction appears to be typical based on previous correlations at Honda R&D.

The conditions shown in Fig. 13 are near the climb condition. The drag coefficients obtained in the low-speed wind tunnel are 4–5 counts lower than those predicted by the Eppler code,[7,8] which is typical based on previous correlations. The MCARF predictions are in good agreement with the test results, and again the MSES code underestimates the drag, in spite of the lower amplification factor of nine selected based on previous correlations with wind-tunnel, not flight, data.

Pitching Moment

Figure 14 shows the section pitching moment coefficients from the flight test and transonic wind-tunnel test. All of the codes overpredict the pitching moment probably because they do not properly account for the small separation on the upper surface at the trailing edge. This separation was modeled by modifying the trailing-edge geometry in the MSES analysis, and the pitching moments then agreed better. This correlation demonstrates that the separation caused by the steep pressure gradient at the trailing edge alleviates the nose-down pitching moment. This is a feature of the SHM-1 design. The constraint on the pitching moment was satisfied.

Effects of Steps and Surface Roughness

Figure 15 shows an example of the effect of a step on the drag obtained from the flight test. The 0.2-mm-high step located at 20% chord on the upper surface causes a drag increase of about 3 counts for $Re < 13 \times 10^6$ and $M = 0.62$. The drag increase is 10 times as

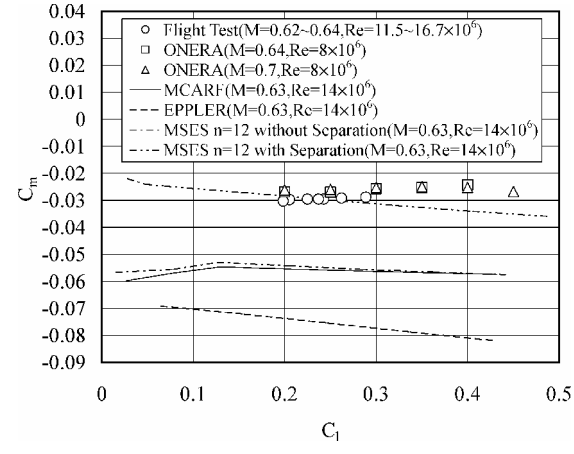

Fig. 14 Comparison of theoretical and experimental (flight and transonic wind tunnel) pitching moment coefficients.

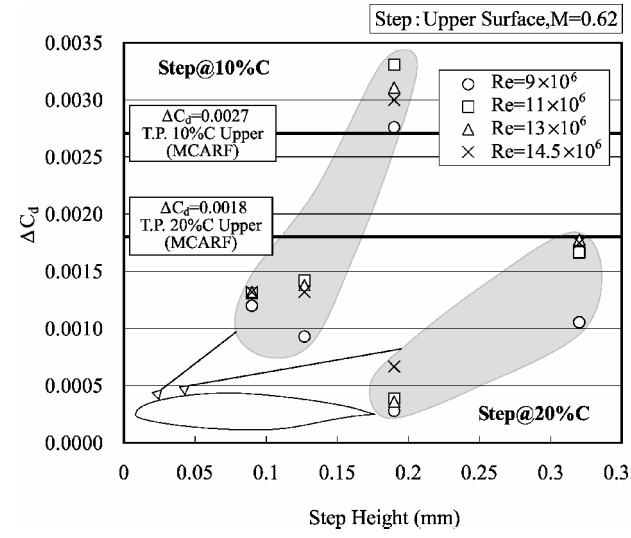

Fig. 15 Effect of step on drag.

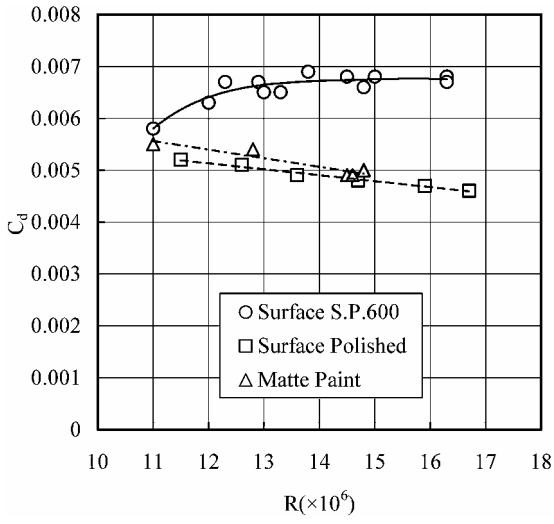

Fig. 16 Effect of surface roughness on drag.

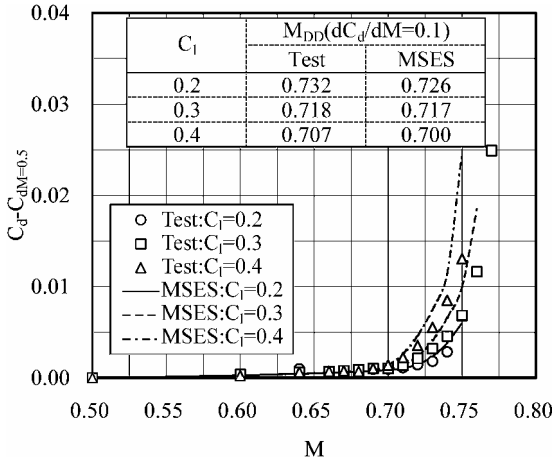

C_l	$M_{DD}(dC_d/dM=0.1)$	
	Test	MSES
0.2	0.732	0.726
0.3	0.718	0.717
0.4	0.707	0.700

Fig. 17 Comparison of theoretical and experimental (transonic wind tunnel)drag-divergence Mach numbers for $Re = 8.0 \times 10^6$ with transition fixed.

great if the same step is located at 10% chord. This result demonstrates that the chordwise location of the step is critical with respect to drag. These data were used to determine the chord location and step-height constraint for the upper-skin parting line for the wing structural design.

Figure 16 shows the effect of surface roughness on the drag. When the surface was sanded with number 600 paper, the drag increased more than 17 counts compared to matte paint surface for $Re \geq 14 \times 10^6$; the drag increase diminished with decreasing Reynolds number. When the surface sanded with number 600 paper was polished with a wax, the drag decreased to the same level as the matte paint surface.

Drag Divergence

Figure 17 shows the drag-divergence characteristics obtained from the transonic wind-tunnel test. The measured drag-divergence Mach numbers are predicted well by the MSES code. The design requirement that M_{DD} be higher than 0.70 at $C_l = 0.38$ was achieved.

Figure 18 shows an example of the shock-wave characteristics of the SHM-1 airfoil at high Mach numbers. The color schlieren technique shows the formation of the shock and the resulting boundary-layer separation. Figure 18a shows a small shock that appears at $M = 0.71$. Figure 18b shows the shock at $M = 0.73$, which is near M_{DD}. The stronger shock at $M = 0.78$ (Fig. 18c) induces separation, and an oscillating shock occurs at $M = 0.80$ (Fig. 18d), which is considered the buffet limit for this airfoil.

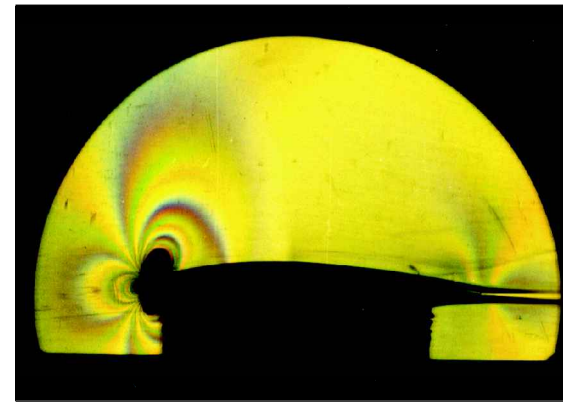

a) Shock appearance $M = 0.71$

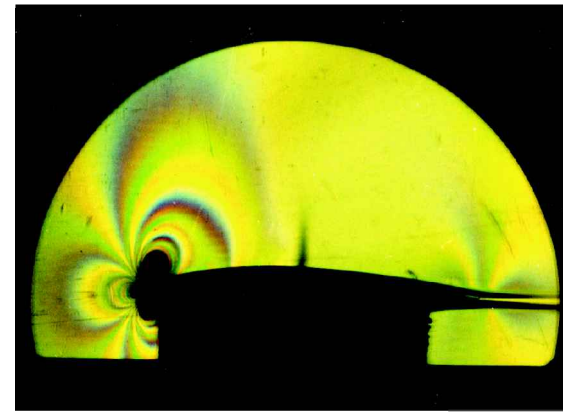

b) Drag-divergence Mach number $M = 0.73$

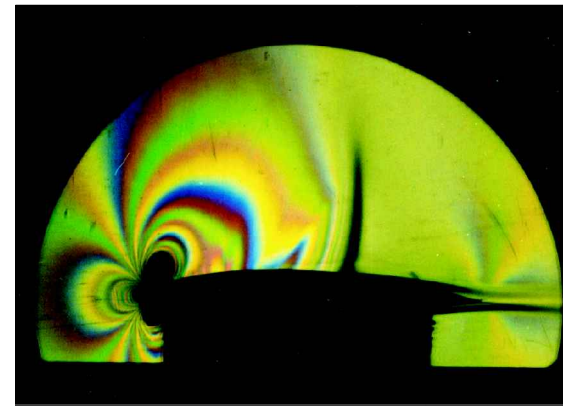

c) Shock-induced separation $M = 0.78$

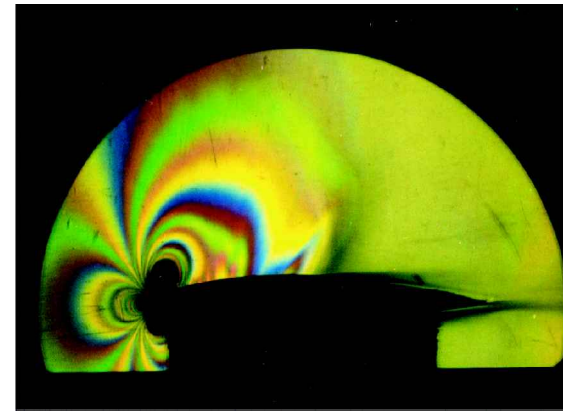

d) Buffet limit $M = 0.8$

Fig. 18 Schlieren photographs, $Re = 8 \times 10^6$ and $\alpha = 0.5$ deg.

Conclusions

An NLF airfoil, the SHM-1, for a lightweight business jet was developed. The airfoil exhibits a high maximum lift coefficient, low profile drag coefficients at climb and cruise, and a small nose-down pitching moment coefficient at high speeds. In addition, the stall characteristics are docile, and the loss in maximum lift coefficient due to leading-edge contamination is small compared with conventional NLF airfoils. All of these characteristics are very important for business-jet applications. The cross-sectional area of the airfoil is about 9% larger than that of the NACA 64_2-215 airfoil and about 16% larger than that of the NASA HSNLF(1)-0213 airfoil; thus, it is possible to carry the required fuel in the wing without increasing the wing size. Therefore, the wing area is minimized by using the SHM-1 airfoil. From extensive flight and low-speed and transonic wind-tunnel tests, the following results were obtained.

1) Representative performance characteristics are as follows.

a) $C_{l\max} = 1.66$ for $Re = 4.8 \times 10^6$ and $M = 0.134$ (low-speed wind tunnel).

b) loss in $C_{l\max}$ due to leading-edge contamination is 5.6% for $Re = 4.8 \times 10^6$ and $M = 0.134$ (low speed wind tunnel).

c) $C_d = 0.0051$ at $C_l = 0.26$ for $Re = 13.2 \times 10^6$ and $M = 0.66$ (flight test), and $C_d = 0.0049$ at $C_l = 0.35$ for $Re = 10.3 \times 10^6$ and $M = 0.27$ (low-speed wind tunnel).

d) $C_m = -0.030$ at $C_l = 0.20$ for $Re = 16.7 \times 10^6$ and $M = 0.64$ (flight test), and $C_m = -0.025$ at $C_l = 0.40$ for $Re = 8.0 \times 10^6$ and $M = 0.70$ (transonic wind tunnel).

e) $M_{DD} > 0.718$ at $C_l = 0.30$ (transonic wind tunnel), and $M_{DD} > 0.707$ at $C_l = 0.40$ (transonic wind tunnel).

2) The drag increase due to a 0.2-mm-high step at 20% chord is about 3 counts for $Re \leq 13 \times 10^6$. The same step placed at 10% chord produces a drag increase of more than 27 counts. The upper-skin parting line and step-height criteria for the actual wing structure were determined based on these results.

3) The prediction of the maximum lift coefficient by the Eppler code[7,8] was in good agreement with the low-speed wind-tunnel results for $Re \geq 4.8 \times 10^6$. The profile drag coefficients predicted by the Eppler code are slightly higher than the experimental values. The MSES code tends to underpredict the profile drag, but its prediction of the drag-divergence Mach number agrees well with the results obtained from the transonic wind-tunnel test. The pressure distributions and shock locations at high speeds predicted by the MSES code agreed well with the flight-test results. The pitching moment coefficients also agreed well if trailing edge separation was modeled by a geometry modification.

4) The in-flight IR imaging technique to visualize boundary-layer transition is a valuable tool. The movement of transition with respect to angle of attack or due to contamination can be observed in real time, which is very helpful for understanding the transition phenomena at various conditions.

Acknowledgments

We thank Honda R&D for permission to publish this paper and colleagues K. Morishita, Y. Wariishi, M. Aoki, J. Sawada, K. Niizuma, A. Ogawa, K. Goto, T. Ide, H. Oyama, and K. Oi for their invaluable assistance. The cooperation of D. Somers of Airfoils Inc., is gratefully acknowledged. Finally, Avtel Services Inc., Fiberset, ONERA Modane-Avrieux Wind Tunnels Department is acknowledged for their cooperation with this research.

References

[1] Abbott, I. H., Von Doenhoff, A. E., and Stivers, L. S., Jr., "Summary of Airfoil Data," NACA Rept. 824, 1945 (supersedes NACA WR L-560).

[2] Somers, D. M., "Subsonic Natural-Laminar-Flow Airfoils," *Natural Laminar Flow and Laminar Flow Control*, edited by R. W. Barnwell and M. Y. Hussaini, Springer-Verlag, New York, 1992, pp. 143–176.

[3] 3McGhee, R. J., Viken, J. K., Pfenninger, W., Beasley, W. D., and Harvey, W. D., "Experimental Results for a Flapped NLF Airfoil with High Lift/Drag Ratio," NASA TM-85788, May 1984.

[4] Viken, J. K., Viken, S. A., Pfenninger, W., Morgan, H. L., Jr., and Campbell, R. L., "Design of the Low Speed NLF(1)-0414F and the High Speed HSNLF(1)-0213 Airfoils with High-Lift Systems," Research in Natural Laminar Flow and Laminar-Flow Control, NASA CP-2487, Pt. 3, 1987, pp. 637–671.

[5] Waggoner, E. G., Campbell, R. L., Phillips, P. S., and Viken, J. K., "Computational Design of Natural Laminar Flow Wings for Transonic Transport Application," Langley Symposium on Aerodynamics, NASA CP-2397, Vol. 1, April 1985, pp. 415–443.

[6] Sewall, W. G., McGhee, R. J., Hahne, D. E., and Jordan, F. L., Jr., "Wind Tunnel Results of the High-Speed NLF(1)-0213 Airfoil," Research in Natural Laminar Flow and Laminar-Flow Control, NASA CP-2487, Pt. 3, 1987, pp. 697–726.

[7] Eppler, R., "Airfoil Program System 'PROFIL97' User's Guide," Ver. 11.6.97, June 1997.

[8] Eppler, R., *Airfoil Design and Data*, Springer-Verlag, Berlin, 1990.

[9] Morgan, H. L., "High-Lift Flaps for Natural Laminar Flow Airfoils," *Laminar Flow Aircraft Certification*, NASA CP-2413, 1986, pp. 31–65.

[10] Drela, M., "A User's Guide to MSES 2.95," MIT Computational Aerospace Sciences Lab., Massachusetts Inst. of Technology, Cambridge, MA, Sept. 1996.

[11] Maughmer, M. D., and Somers, D. M., "Design and Experimental Results for a High-Altitude, Long-Endurance Airfoil," *Journal of Aircraft*, Vol. 26, No. 2, 1989, pp. 148–153.